Artvin Çoruh Üniversitesi
Orman Fakültesi Dergisi
ISSN:2146-1880, e-ISSN: 2146-698X
Yıl: 2025, Cilt: 26, Sayı: 1, Sayfa: 202-211

ofd.artvin.edu.tr

Artvin Coruh University
Journal of Forestry Faculty
ISSN:2146-1880, e-ISSN: 2146-698X
Year: 2025, Vol: 26, Issue: 1, Pages:202-211

Thermal properties of nanofibrillated cellulose/PMMA/MMA/benzoyl peroxide-reinforced transparent epoxy nanocomposites

Nanofibril selüloz/PMMA/MMA/benzoil peroksit takviyeli şeffaf epoksi nanokompozitlerin termal özellikleri

Mert YILDIRIM*[1,2]

1 Istanbul Gelisim University, Faculty of Engineering and Architecture, Department of Industrial Engineering, Istanbul, Türkiye

2 Istanbul Gelisim University, New Generation Entrepreneurship and Innovation Application and Research Center, Istanbul, Türkiye

Eser Bilgisi/*Article Info*
Araştırma makalesi/*Research article*
DOI: 10.17474/artvinofd.1646742

Sorumlu yazar/*Corresponding author*
Mert YILDIRIM
e-mail: meryildirim@gelisim.edu.tr

Geliş tarihi/*Received*
25.02.2025
Düzeltme tarihi/*Received in revised form*
09.05.2025
Kabul tarihi/Accepted
09.05.2025
Elektronik erişim/*Online available*
15.05.2025

Keywords:
Thermal properties
Transparent epoxy nanocomposites
Nanocellulose
PMMA

Anahtar kelimeler:
Termal özellikler
Şeffaf epoksi nanokompozitler
Nanoselüloz
PMMA

Abstract

This study presents the synergistic effects of nanofibrillated cellulose (NFC), polymethyl methacrylate (PMMA), methyl methacrylate (MMA), and benzoyl peroxide (BPO) additives on the thermal properties of nanocomposites. The nanocomposites were fabricated by the casting method through the incorporation of 1%, 3%, and 5% NFC, 0.05% PMMA and MMA, and 0.005% BPO into epoxy resin. The results of the thermal analysis indicate that the thermal stability, residue content, storage modulus (E'), loss modulus (E''), and tan delta (Tan δ) values of all reinforced nanocomposites significantly increased compared to the neat epoxy samples. The findings demonstrate that the nanocomposites containing 3% NFC, 0.05% PMMA and MMA, and 0.005% BPO exhibited superior thermal resistance and stability, along with the highest storage modulus, loss modulus, and tan delta values. Based on the obtained results, it was determined that a 3% NFC loading is the most optimal ratio for enhancing the thermal properties of sustainable transparent nanocomposites, making these materials suitable for advanced material applications.

Özet

Bu çalışma, nanofibril selüloz (NFC), polimetil metakrilat (PMMA), metil metakrilat (MMA) ve benzoil peroksit (BPO) katkı maddelerinin nanokompozitlerin termal özellikleri üzerindeki sinerjik etkilerini sunmaktadır. Nanokompozitler, epoksi reçine içerisine %1, %3 ve %5 oranında NFC ilavesi, %0.05 oranında PMMA ve MMA ilavesi ve %0.005 oranında BPO ilavesi katılarak döküm yöntemiyle üretilmiştir. Yapılan termal analizin sonuçları, tüm takviyeli nanokompozitlerin termal kararlılığının, kalıntı içeriğinin, depolama modülünün (E'), kayıp modülünün (E'') ve tan delta (Tan δ) değerlerinin saf epoksili örneklere kıyasla önemli ölçüde arttığını göstermektedir. Bulgular, %3 NFC, %0.05 PMMA ve MMA ile %0.005 BPO içeren nanokompozitlerin üstün termal direnç ve kararlılık sergilediğini ve bu nanokompozitlerin en yüksek depolama modülü, kayıp modülü ve tan delta değerlerine sahip olduğunu göstermektedir. Elde edilen sonuçlara göre, sürdürülebilir şeffaf nanokompozitlerin termal özelliklerini iyileştirmek amacıyla özellikle %3 NFC yüklemesinin en uygun oran olduğu belirlenmiş ve yüklemenin bu malzemeleri ileri düzey malzeme uygulamaları için uygun hale getirdiği sonucuna varılmıştır.

INTRODUCTION

Nowadays, the efficient utilization of biologically sourced raw materials and the production of various products from these sources have become a major focus of interest. Due to their relatively availability, sustainability, and renewability, lignocellulosic biomass resources stand out. Lignocellulosic biomass is composed of cellulose, lignin, and hemicellulose. It has attracted attention as a potential alternative to fossil-derived products such as fuels and chemicals and is recognized as a valuable renewable resource for the production of bio-based polymers and materials. The global production of lignocellulosic biomass is estimated to reach approximately 181.5 billion tons per year (Lee et al. 2023). Cellulose is the most plentiful lignocellulosic biomaterial in nature (Dufresne 2017). In contrast, nanocellulose is an bionanomaterial with exceptional characteristics, produced by breaking down cellulose fibers into nanoscale dimensions (Candan et al. 2022). Due to its unique characteristics, nanocellulose has become increasingly popular in various industries in recent years (Yildirim et al. 2024a).

In recent years, various transparent polymers, especially poly(methyl methacrylate) (PMMA), have become more

popular because of their outstanding optical clarity and low density (Kumari et al. 2024). PMMA is extensively used in various industries due to its transparency, high transmittance, and lightweight (Chen et al. 2018, Radhi et al. 2021, Saxena and Shukla 2022). However, despite its significant potential, PMMA has some limitations, including suboptimal mechanical and dynamic properties, which limit its use in engineering applications (Liu et al. 2010). To address these challenges, the incorporation of nano-fillers as reinforcement has been suggested (Nussbaumer et al. 2003, Chen et al. 2009, Tang and Weder 2010).

Thermal analysis methods provide comprehensive data about a material's thermal properties, stability, and reactions to temperature changes (Gill et al. 2010, Gabr et al. 2014, Saba et al. 2016, Saba et al. 2017). Thermal analysis are vital in materials science as they offer valuable insights into the thermal behavior and stability of materials, which is essential for evaluating and enhancing their performance under different conditions (Yildirim et al. 2024b). This information is crucial for choosing materials in industries like aerospace, automotive, and electronics.

Many studies in recent years have focused on the thermal analysis of epoxy nanocomposites reinforced with nanocellulose derived from various cellulosic sources (Gan et al. 2020, Subbotina et al. 2022, Barra et al. 2023, Kumar et al. 2024, Manimaran et al. 2024, Yusuf et al. 2024). Nonetheless, these composites have limited applicability in advanced material areas.

In our previous study, we investigated the synergistic effects of nanofibrillated cellulose/PMMA-MMA-BPO on the mechanical and self healing properties of nanocomposites (Yildirim and Candan 2024). This study aims to assess the combined effects of incorporating NFC, PMMA, MMA, and BPO into epoxy at various concentrations to improve thermal stability, char yield, glass transition temperature, as well as the elastic, viscous, and compliance properties of the composites.

MATERIAL AND METHOD

Material

The epoxy resin and hardener were sourced from Armor Chemical. The NFCs obtained from wood pulp using the 2,2,6,6,6-tetramethylpiperidin-1-yl-oxy (TEMPO) method were used. The NFCs have a diameter of 20 nm and a length of 1 micron. PMMA (with the linear formula $[CH_2C(CH_3)(CO2CH_3)]$), MMA (with the linear formula $CH_2=C(CH_3)COOCH_3$), and BPO (with the empirical formula $C_{14}H_{10}O_4$) were purchased from Sigma-Aldrich.

Method

The epoxy and hardener were mixed in a 2:1 weight ratio. The NFC was added to the resin at weight ratios of 1%, 3%, and 5% relative to the prepared epoxy solution, and mixed using a ultrasonic homogenizer at 2000 rpm for 5 minutes.

In a cardboard cup, 0.005% BPO and 0.05% PMMA, by weight of the epoxy mixture, were mixed. In a cardboard cup, 0.005% MMA and 0.05% PMMA, both based on the weight of the epoxy mixture, were mixed. Half of the epoxy solution containing NFC was added to the cup with BPO, and the other half was added to the cup with MMA. Each mixture was separately mixed in a ultrasonic homogenizer at 2000 rpm for 5 minutes to obtain a homogenous consistency. The three mixtures were then combined into a single container, and the final polymer solution was prepared by mixing in the sonicator at 2000 rpm for 5 minutes until fully homogeneous. The mixture was poured to a PTFE panel and left to cure for 72 hours at room temperature. A comparable method was employed to prepare control samples made of pure composites with no additives.

Table 1 presents the experimental design for both the unreinforced and reinforced samples.

Table 1. Experimental design of this study

Sample ID	NFC (%)	PMMA (%)	MMA (%)	BPO (%)
Control	0	0	0	0
D	1	0.05	0.05	0.005
E	3	0.05	0.05	0.005
F	5	0.05	0.05	0.005

Thermal Analyses of Nanocomposites

Thermogravimetric Analysis

The TGA analysis was performed using a Hitachi (Japan) TG/DTA analyzer located in the Nanotechnology and Thermal Analysis Laboratory at Istanbul University-Cerrahpasa. 5 mg of the sample was heated from room temperature to 800°C at a heating rate of 10°C/min. Nitrogen gas (N2) was used as an inert purge gas to prevent unwanted oxidation of the materials. Additionally, the rate of weight loss as a function of time was determined using derivative thermogravimetric (DTG) curves.

Differential Scanning Calorimetry

The DSC analysis was also conducted using a Hitachi (Japan) DSC analyzer in the same laboratory. 5 mg of each sample was placed in an aluminum pan and heated from 30°C to 200°C at a rate of 10°C/min. The gas flow rate was set to 30 ml/min.

Dynamic Mechanical Thermal Analysis

Within the scope of DMTA analysis, the storage modulus (E'), loss modulus (E''), and tan delta (δ) were analyzed. The DMTA analysis was carried out using a Hitachi (Japan) DMTA analyzer, also located in the same laboratory. The sample dimensions were 50 mm × 10 mm × 3 mm, and all samples were tested at a frequency of 1 Hz. The temperature was increased from -50°C to 200°C at a heating rate of 5°C/min.

RESULTS AND DISCUSSION

Thermogravimetry Analysis

The thermal degradation curve for both unreinforced and reinforced samples as the temperature increases is shown in Figure 1.

As shown in Figure 1, the X-axis shows the temperature to which the material was exposed during the TGA analysis, while the Y-axis shows the percentage of mass remaining as the temperature increases.

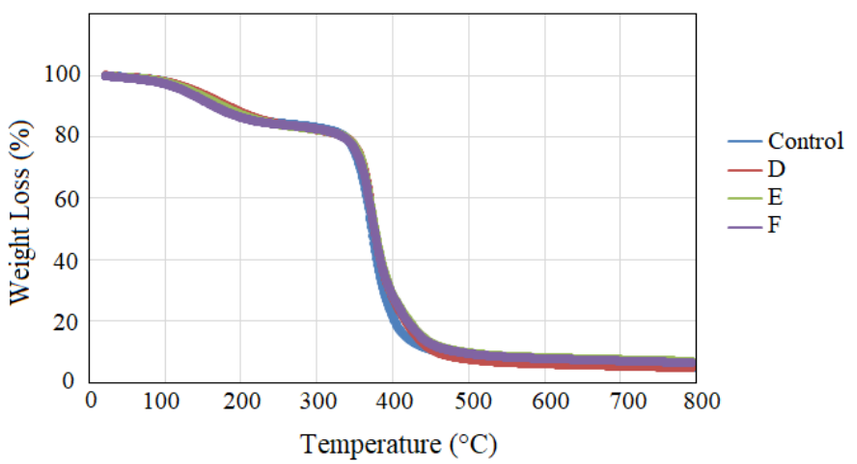

Figure 1. TGA curves for both unreinforced and reinforced samples

Both the control and reinforced groups showed similar thermal behavior at low temperatures. There was a minimum weight loss of about 2-5% up to about 100°C. This can be attributed to the first degradation observed below 150°C, which is primarily due to the evaporation of surface-adsorbed moisture, volatile components within

the composites, and the dehydration of alcohol groups present in the epoxy. A significant weight loss occurred between 300°C and ~500°C. The weight loss in this area has reached approximately 70–80%. This is where the bulk of the decomposition occurs, indicating that a significant thermal event, such as the breakdown of organic components or volatilization of certain compounds, occurs in this temperature range.

The second decomposition occurring at 300°C is related to three factors. The first is the simultaneous decomposition of glycosidic bonds in cellulose, the second is the degradation of aromatic groups in epoxy, and the third is the degradation of aliphatic amine groups in curing compounds (Sen and Kumar 2010, Lee et al. 2012, Wu et al. 2015). After 500°C, the curves stabilized. No significant weight loss occurred beyond this temperature. This suggests that the majority of the volatile components have already vanished. Beyond 400°C, degradation continued gradually up to 800°C with only small decreases in weight. At 800°C, the residual weight of all groups stabilized around 0-10%. The residual content at 800°C was measured from the TG analysis and expressed as a percentage. The control group had a 4% residue, while group D showed 5%, group E had 7%, and group F observed 6%.

In comparison to the control samples, the reinforced samples generally show noticeably higher degradation temperatures and better thermal stability. Especially, groups D, E, and F displayed reduced thermal degradation, as evidenced by the shift of the temperature at which maximum weight loss occurs to a higher value, moving further along the temperature scale.

Similar trends have been reported by other researchers (Qua et al. 2009, Saba et al. 2017, Pandurangan and Kanny 2020).

Derivative Thermogravimetry

Figure 2 presents the DTG curves for both unreinforced and reinforced samples as the temperature increases, the derivative of mass loss per unit temperature.

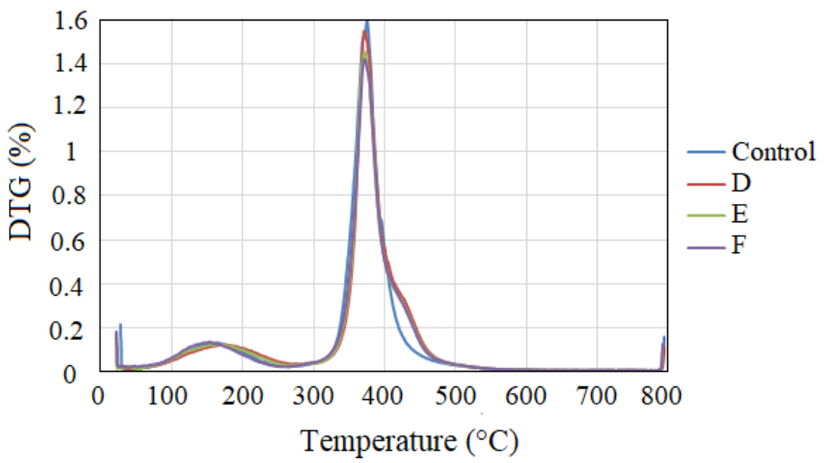

Figure 2. DTG curves for both unreinforced and reinforced samples

As illustrated in Figure 2, all groups showed a similar thermal degradation pattern. The most prominent degradation event occurred between 350°C and 400°C, where a major peak was evident for each group. Slight changes in peak intensity were observed, particularly around 375°C. Samples D, E, and F showed slightly lower peak heights compared to the control group. This reduction is likely due to a small decrease in the mass loss rate, indicating improved thermal stabilization. The control group's highest point was 1.59, while groups B, C, and A recorded peak heights of 1.55, 1.45, and 1.42, respectively. All the reinforced groups exhibited slower degradation rates compared to the control.

Differential Scanning Calorimetry

Figure 3 presents the DSC curves for both unreinforced and reinforced samples as the temperature increases.

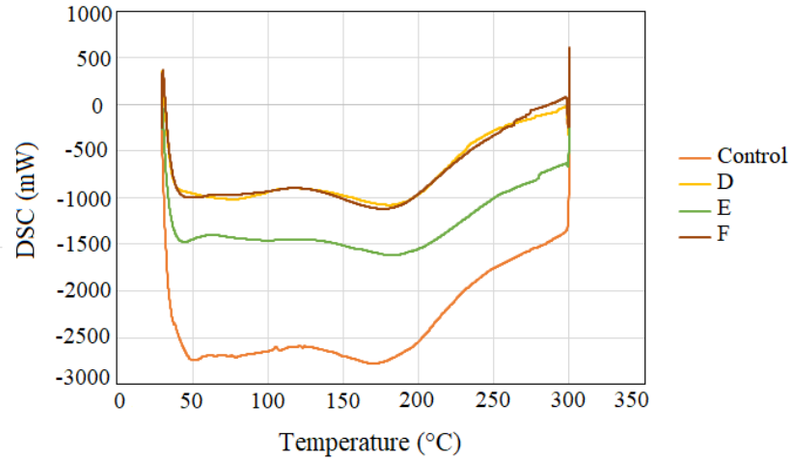

Figure 3. DSC curves for both unreinforced and reinforced samples

As demonstrated in Figure 3, the control group exhibited a clear endothermic peak around 50°C, followed by a relatively stable heat flow until about 200°C. The endothermic change that occurs between 150°C and 230°C is connected with the removal of water owing to dehydration of the secondary alcohol group (Saba et al. 2017). Between 200°C and 300°C, the control group displayed a gradual increase in heat flow, indicating thermal degradation or another exothermic event occurring above 300°C. Epoxy resins are endothermic up to 250°C before becoming exothermic (Saba et al. 2017). Other studies have reported similar results (Xu et al. 2013).

Group D shows a similar pattern to the control group. However, it has slightly lower endothermic values in the initial region below 100°C. The heat flow profile between 100°C and 300°C shows a gradual upward shift compared to the control group. This indicates that Group D exhibits improved thermal stability compared to the control group.

Group E showed a similar endothermic transition near 50°C. However, the magnitude of the heat flux was lower compared to the control group and Group D. Between 100°C and 250°C, the heat flow remains more consistent. This indicates a higher thermal stability. Above 250°C, there is a slight increase in heat flow, but it is lower than in the control group. This indicates lower thermal degradation.

Group F showed the lowest endothermic heat flow of all samples below 100°C. Group F showed a consistent heat flow profile from 100°C to 300°C, slightly lower than the other samples, indicating the highest thermal stability. After 300°C, there is a noticeable increase in heat flow. This indicates delayed or reduced thermal degradation compared to the control group.

In general, groups D, E, and F showed lower endothermic heat flux in the initial stages compared to the control group. Group F in particular shows the most significant shift towards improved thermal stability, as evidenced by relatively lower heat flux and delayed degradation across the temperature range. This indicates potential improvements in thermal resistance or changes in the polymeric structure leading to slower degradation. The incorporation of NFC into epoxy enhances the Tg value of the epoxy resin by limiting the movement of polymer chains through physical or chemical interactions. The Tg values of the reinforced samples increased compared to the control group. This is because adding reinforcing material to a polymer matrix decreases chain mobility within the composite material (Saba et al. 2017, Hamou et al. 2018).

Storage Modulus

Figure 4 presents the storage modulus (E') curves for both unreinforced and reinforced samples.

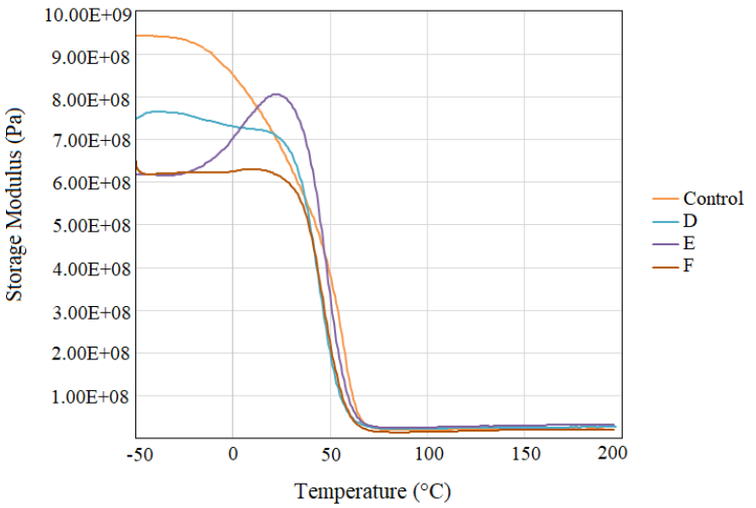

Figure 4. E' curves for both unreinforced and reinforced samples

As can be seen in Figure 4, the E' value decreases sharply as the temperature increases toward the glass transition temperature (Tg). This decrease was observed for all samples between approximately 50°C and 100°C. This decrease is related to the transition from the glassy to the rubbery state, where the polymer chain mobility increases, leading to a decrease in material stiffness.

The control group shows a sharp decrease of the E' after the glass transition, from a value of about 7.0×10E+08 Pa in the glassy state to below 1.0×10E+08 Pa in the rubbery state. Group D followed a similar trend with the control group. However, it showed a slightly higher modulus in the glassy region, peaking at about 7.5×10E+08 Pa before decreasing in the rubbery region. Group E exhibited a notable peak in storage modulus around the glassy transition, reaching a maximum value above 8.0×10E+08 Pa, attributed to a possible reinforcement effect or increased crosslinking compared to the control group. The modulus then decreased after Tg. Group F followed a trend closer to the control group with a storage modulus around 7.0×10E+08 Pa at low temperatures. However, it showed a more gradual decrease after Tg. It maintained higher modulus values in the rubbery region compared to the control and other groups.

Table 2 presents the E'results of the samples at different temperatures.

Table 2. E' results for both unreinforced and reinforced samples.

Sample ID	30°C Pascal (Pa)	50°C Pascal (Pa)	100°C Pascal (Pa)	150°C Pascal (Pa)	200°C Pascal (Pa)
Control	6.30E + 08	3.77E + 08	2.13E + 07	2.48E + 07	2.60E + 07
D	6.68E+08	2.05E+08	2.40E + 07	2.61E + 07	2.70E + 07
E	7.81E+08	3.16E+08	2.64E + 07	3.03E + 07	3.37E + 07
F	5.90E+08	2.10E+08	1.58E+07	2.04E+07	2.14E+07

The control group demonstrates a significant reduction in storage modulus from 30°C to 100°C, as epoxy provides a low level of stiffness (Abdul Khalil et al. 2013). This suggests a considerable decline in hardness at elevated temperatures. However, beyond 100°C, the change becomes less pronounced. Group D behaves similarly to the control group but shows slightly better performance at higher temperatures, particularly at 200°C. Group E starts with the highest storage modulus and exhibits the smallest decrease at higher temperatures, indicating it maintains the highest storage modulus among the groups. Group F experiences a faster decline in modulus with rising temperature compared to the other groups, especially at temperatures above 100°C, suggesting it has poorer thermal stability. Increasing NFC loading to 5% significantly enhances the molecular/segmental movement and rotational motion of epoxy, leading to the deposition of filler particles and the creation of many

empty spaces and voids in the polymer network (Putz et al. 2008, Saba et al. 2017). As a result, both E' and Tg values decrease.

Other researchers reported relatively similar trends and agreements (Chen et al. 2009, Ocando et al. 2010, Kiziltas et al. 2011, Kowalczyk et al. 2011, Erbas Kiziltas et al. 2015).

Loss Modulus

Loss Modulus (E'') curves were recorded as a function of temperature (°C), and the results are shown in Figure 5.

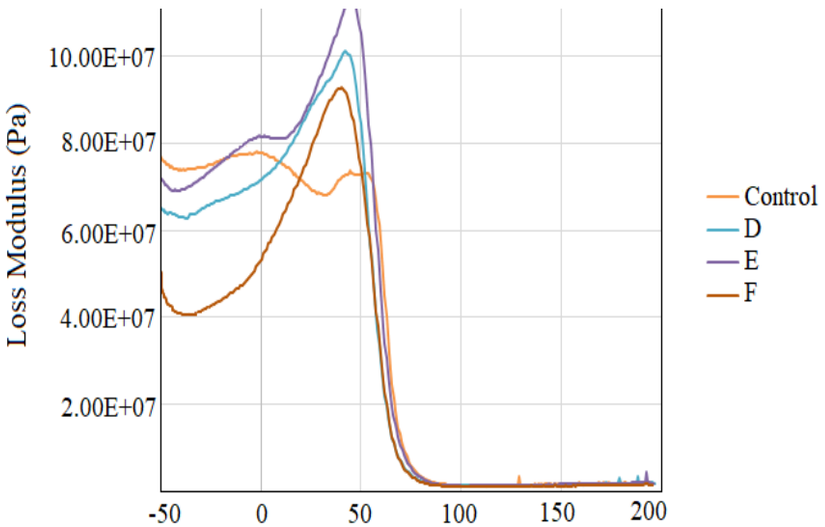

Figure 5. E'' curves for both unreinforced and reinforced samples

According to Figure 5, the control group showed a maximum loss modulus of approximately 55°C, indicating the polymer matrix's typical Tg. A similar peak was seen in group D, although the maximum loss modulus was significantly lower, with a Tg close to the control at roughly 55°C. The general form of the curve implies modest changes in the polymer's dissipative behavior, which could be attributable to the filler's nature or alteration. Group E showed the highest peak in loss modulus, indicating the most energy dissipation during the glass transition. The Tg for this sample was near 60°C, somewhat higher than the control, indicating an increase in stiffness or cross-link density inside the polymer network. The loss modulus peak for group F was lower than that of the control, occurring at roughly 50°C. The drop in both the peak value and Tg could indicate a plasticizing impact, resulting in lower energy dissipation and an earlier commencement of the glass transition.

Across all samples, the loss modulus drops significantly after Tg, as expected, due to the transition to the rubbery state of the material at higher temperatures. Minimal deviations in the post-transition regions indicate consistent behavior at elevated temperatures for all samples.

Table 3 presents results to the E'' of samples across various temperature ranges.

Table 3. E'' values for both unreinforced and reinforced samples

Sample ID	30°C Pascal (Pa)	50°C Pascal (Pa)	100°C Pascal (Pa)	150°C Pascal (Pa)	200°C Pascal (Pa)
Control	6.30E+08	3.77E+08	2.13E+07	2.48E+07	2.60E+07
D	9.24E+07	8.10E+07	1.32E+06	1.49E+06	1.84E+06
E	9.59E+07	1.03E+08	1.22E+06	1.58E+06	1.85E+06
F	8.56E+07	7.21E+07	1.05E+06	1.20E+06	1.35E+06

As can be seen in Table 3, all groups showed a significant decrease in storage modulus between 30°C and 100°C, followed by a slight increase from 100°C to 200°C. This reflects the common behavior of many materials, where higher temperatures lead to reduced energy dissipation and lower viscous resistance. The control group shows a significantly higher loss modulus across all temperatures compared to groups D, E, and F. This indicates that the modifications applied to D, E, and F reduce the composites ability to dissipate energy through viscous forces.

Tan Delta

Figure 6 presents the tan δ curves for both the unreinforced and reinforced samples.

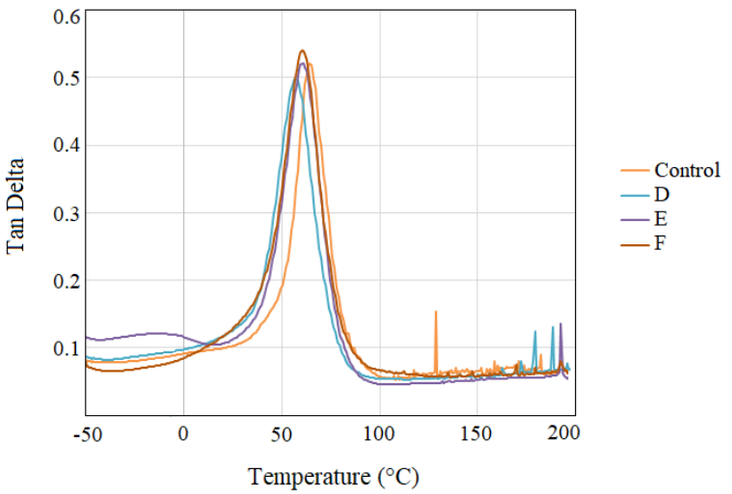

Figure 6. Tan δ curves for both unreinforced and reinforced samples

A peak in tan δ signifies the glass transition temperature (Tg). As shown in Figure 6, all samples exhibit a clear peak within the range of 50°C to 70°C, corresponding to their individual Tg values. The peak positions vary slightly across each group, indicating that the type of additives and their concentrations influence the glass transition temperatures of the materials.

Table 4 presents the Tg values for both unreinforced and reinforced samples.

Table 4. Tg results from Tan δ for both unreinforced and reinforced samples.

Sample ID	Tg (°C)
Control	64.1
D	58.1
E	61.9
F	61.2

The magnitude of the Tan δ peak gives information about the damping properties of the material. The peak of the tan δ corresponds to the Tg value of each sample. For the control group, Tg was observed at 64.1°C, as indicated by the sharp rise in Tan δ. According to Table 4, Tg values were recorded at 58.1°C in group D, 61.9°C in group E, and 61.2°C in group F.

The control group achieved a higher peak height compared to the reinforced groups. This difference may result from two factors: epoxy possesses greater molecular mobility, and the reinforcing materials reduce epoxy's viscoelastic damping factor (Yildirim et al. 2024b). This also indicates that the unreinforced sample has a greater ability to dissipate energy in the glass transition region. The smaller peaks for the reinforced samples are likely a result of changes in molecular mobility or interactions, possibly due to crosslinking. The broader peaks in groups D, E, and F indicate a more gradual transition, in contrast to the sharper transition observed in the control group. The slight shift in Tg and the reduction in tan δ values for the reinforced samples point

to alterations in the viscoelastic properties of the polymer matrix.

Increased NFC level from 1% to 3% resulted in higher Tg values. However, at a 5% loading level, Tg was slightly decreased. At 5% and greater loadings, the strength of tan δ peaks decreases due to slower agglomeration and energy dissipation with NFC (Chen et al. 2008, Saba et al. 2017, Yildirim et al. 2024b).

CONCLUSION

The results clearly demonstrate that the addition of NFC/PMMA/MMA/BPO additives substantially enhances the thermal stability and dynamic mechanical properties of the nanocomposites compared to the control group. The results indicate that even at low loading levels of NFC, PMMA, MMA, and BPO, enhanced thermal properties can be achieved.

Group E showed the highest degradation temperatures and the greatest improvement in thermal stability, along with superior storage modulus (E') and loss modulus (E'') across the entire temperature range relative to the other reinforced groups. Overall, nanocomposites containing 3% NFC, 0.05% PMMA, 0.05% MMA, and 0.005% BPO fillers showed the most favorable combination of thermal stability and viscoelastic performance. However, when the NFC content exceeds 5%, a marked decrease in both thermal stability and dynamic mechanical properties is observed.

From an industrial perspective, the enhanced thermal stability makes these transparent nanocomposites suitable candidates for aerospace structures and automotive components. Due to their transparency, improved thermal stability, these materials may serve in substrates for electronic circuits, LED encapsulations, and sensor applications.

ACKNOWLEDGMENTS

The author expresses gratitude to the Turkish Academy of Sciences and the Biomaterials and Nanotechnology Research Group.

REFERENCES

Abdul Khalil HPS, Jawaid M, Firoozian P, Zainudin ES, Paridah MT (2013) Dynamic mechanical properties of activated carbon–filled epoxy nanocomposites. Int J Polym Anal Charact, 18(4): 247-256.

Barra G, Guadagno L, Raimondo M, Santonicola MG, Toto E, Vecchio Ciprioti SA (2023) Comprehensive review on the thermal stability assessment of polymers and composites for aeronautics and space applications. Polymers, 15: 3786.

Candan Z, Tozluoglu A, Gonultas O, Yildirim M, Fidan H, Alma MH, Salan T (2022) Nanocellulose: Sustainable Biomaterial for Developing Novel Adhesives and Composites. In: Sapuan SM, Norrrahim MNF, Ilyas RA, Soutis C (eds) Industrial Applications of Nanocellulose and Its Nanocomposites, Woodhead Publishing, Sawston, UK, pp. 49-137.

Chen G, Wei M, Chen J, Huang J, Dufresne A, Chang PR (2008) Simultaneous reinforcing and toughening: new nanocomposites of waterborne polyurethane filled with low loading level of starch nanocrystals. Polymer, 49(7): 186-1870.

Chen LS, Huang ZM, Dong GH, He CL, Liu L, Hu YY, Li Y (2009) Development of a transparent PMMA composite reinforced with nanofibers. Polym Compos, 30(3): 239-247.

Chen Y, Cai T, Dang B, Wang H, Xiong Y, Yao Q, Wang C, Sun Q, Jin C (2018) The properties of fibreboard based on nanolignocelluloses/CaCO3/PMMA composite synthesized through mechano-chemical method. Sci Rep, 8(1): 5121.

Dufresne A (2017) Cellulose nanomaterial reinforced polymer nanocomposites. Curr Opin Colloid Interface Sci, 29: 1-8.

Erbas Kiziltas E, Kiziltas A, Bollin SC, Gardner DJ (2015) Preparation and characterization of transparent PMMA–cellulose-based nanocomposites. Carbohydr Polym, 127: 381-389.

Gabr MH, Phong NT, Okubo K, Uzawa K, Kimpara I, Fujii T (2014) Thermal and mechanical properties of electrospun nanocelullose reinforced epoxy nanocomposites. Polym Test, 37: 51-58.

Gan PG, Sam ST, Abdullah MF, Omar MF (2020) Thermal properties of nanocellulose-reinforced composites: a review. J Appl Polym Sci, 137(11): 48544.

Gill P, Moghadam TT, Ranjbar B (2010) Differential scanning calorimetry techniques: applications in biology and nanoscience. J Biomol Tech, 21(4): 167-193.

Hamou KB, Kaddami H, Dufresne A, Boufi S, Magnin A, Erchiqui F (2018) Impact of TEMPO-oxidization strength on the properties of cellulose nanofibril reinforced polyvinyl acetate nanocomposites. Carbohydr Polym, 181: 1061-1070.

Kiziltas A, Gardner DJ, Han Y, Yang HS (2011) Dynamic mechanical behavior and thermal properties of microcrystalline cellulose (MCC)-filled nylon 6 composites. Thermochim Acta, 519(1-2): 38-43.

Kowalczyk M, Piorkowska E, Kulpinski P, Pracella M (2011) Mechanical and thermal properties of PLA composites with cellulose nanofibers and standard size fibers. Compos Part A Appl Sci Manuf, 42(10): 1509-1514.

Kumar B, Adil S, Pham DH, Kim J (2024) Environment-friendly, high-performance cellulose nanofiber-vanillin epoxy nanocomposite with excellent mechanical, thermal insulation and UV shielding properties. Heliyon, 10(3): e25272.

Kumari S, Mishra RK, Parveen S, Avinashi SK, Hussain A, Kumar S, Banerjee M, Rao J, Kumar R, Gautam RK, Gautam C (2024) Fabrication, structural, and enhanced mechanical behavior of MgO substituted PMMA composites for dental applications. Sci Rep, 14: 2128.

Lee J, Kim S, You S, Park YK (2023) Bioenergy generation from thermochemical conversion of lignocellulosic biomass-based integrated renewable energy systems. Renew Sustain Energy Rev, 178: 113240.

Lee KY, Tammelin T, Schulfter K, Kiiskinen H, Samela J, Bismarck A (2012) High performance cellulose nanocomposites: comparing the reinforcing ability of bacterial cellulose and nanofibrillated cellulose. ACS Appl Mater Interfaces, 4(8): 4078-4086.

Liu HY, Liu DG, Yao F, Wu QL (2010) Fabrication and properties of transparent polymethylmethacrylate/cellulose nanocrystals composites. Bioresource Technol, 101 (14): 5685-5692.

Manimaran M, Norizan M, Kassim M, Adam M, Norrrahim M, Knight V (2024) Critical assessment of the thermal stability and degradation of chemically functionalized nanocellulose-based polymer nanocomposites. Nanotechnol Rev, 13(1): 20240005.

Nussbaumer RJ, Caseri WR, Smith P, Tervoort T (2003) Polymer TiO2 nanocomposites: a route towards visually transparent broadband UV filters and high refractive index materials. Macromol Mater Eng, 288(1): 44-49.

Ocando C, Tercjak A, Mondragon I (2010) Nanostructured systems based on SBS epoxidized triblock copolymers and well-dispersed alumina/epoxy matrix composites. Compos Sci Technol, 70(7): 1106-1112.

Pandurangan MT, Kanny K (2020) Study of curing characteristics of cellulose nanofiber-filled epoxy nanocomposites. Catalysts, 10: 831.

Putz KW, Palmeri MJ, Cohn RB, Andrews R, Brinson LC (2008) Effect of cross-link density on ınterphase creation in polymer nanocomposites. Macromolecules, 41(18): 6752-6756.

Qua EH, Hornsby PR, Sharma HSS, Lyons G, McCall RD (2009) Preparation and characterization of poly(vinyl alcohol) nanocomposites made from cellulose nanofibers. J Appl Polym Sci 113(4): 2238-2247.

Radhi A, Mohamad D, Rahman FS, Abdullah AM, Hasan H (2021) Mechanism and factors influence of graphene-based nanomaterials antimicrobial activities and application in dentistry. J Mater Res Tech, 11: 1290-1307.

Saba N, Paridah MT, Abdan K, Ibrahim NA (2016) Dynamic mechanical properties of oil palm nano filler/kenaf/epoxy hybrid nanocomposites. Constr Build Mater, 124: 133-138.

Saba N, Safwan A, Sanyang ML, Mohammad F, Pervaiz M, Jawaid M, Alothman OY, Sain M (2017) Thermal and dynamic mechanical properties of cellulose nanofibers reinforced epoxy composites. Int J Biol Macromol, 102: 822-828.

Saxena P, Shukla PA (2022) A comparative analysis of the basic properties and applications of poly (vinylidene fluoride) (PVDF) and poly (methyl methacrylate) (PMMA). Polym Bull, 79(8): 5635-5665.

Sen AK, Kumar S (2010) Coir-fiber-based fire retardant nano filler for epoxy composites. J Therm Anal Calorim, 101: 265-271.

Subbotina E, Montanari C, Olsén P, Berglund LA (2022) Fully bio-based cellulose nanofiber/epoxy composites with both sustainable production and selective matrix deconstruction towards infinite fiber recycling systems. J Mater Chem, A (10): 570-576.

Tang L, Weder C (2010) Cellulose whisker/epoxy resin nanocomposites. ACS Appl Mater Interfaces, 2(4): 1073-1080.

Wu G, Liu D, Liu G, Chen J, Huo S, Kong Z (2015) Thermoset nanocomposites from waterborne bio-based epoxy resin and cellulose nanowhiskers. Carbohydr Polym, 127: 229-235.

Xu S, Girouard N, Schueneman G, Shofner ML, Meredith JC (2013) Mechanical and thermal properties of waterborne epoxy composites containing cellulose nanocrystals. Polymer, 54 (24): 6589-6598.

Yildirim M, Mutlu I, Candan Z (2024a) Development and characterization of smart composites reinforced with fibrillated cellulose and nickel-titanium alloy. Int J Biol Macromol, 267: 131189.

Yildirim M, Mutlu I, Candan Z (2024b) Thermal properties of cellulose nanofibrils and nickel-titanium alloy-reinforced sustainable smart composites. Wood Mater Sci Eng, 19(3): 557-563.

Yildirim M, Candan Z (2024) Preparation and characterization of transparent advanced smart nanocomposites reinforced by nanofibrillated cellulose/poly(methyl methacrylate)/methyl methacrylate/benzoyl peroxide. Bioresources, 19(3): 5435-5449.

Yusuf J, Sapuan SM, Rashid U, Ilyas RA, Hassan MR (2024) Thermal, mechanical, and morphological properties of oil palm cellulose nanofibril reinforced green epoxy nanocomposites. Int J Biol Macromol, 278(3): 134421.